PRAMANA
— journal of
physics

Vol. 65, No. 4
October 2005
pp. 581–592

Synthesis, characterizations and applications of some nanomaterials (TiO_2 and SiC nanostructured films, organized CNT structures, ZnO structures and CNT–blood platelet clusters)

O N SRIVASTAVA[1,*], A SRIVASTAVA[1], D DASH[2], D P SINGH[1], R M YADAV[1], P R MISHRA[1] and J SINGH[1]

[1]Department of Physics, Banaras Hindu University, Varanasi 221 005, India

[2]Department of Biochemistry, Institute of Medical Sciences, Banaras Hindu University, Varanasi 221 005, India

*Corresponding author. E-mail: hepons@yahoo.com

Abstract. TiO_2 nanostructured films have been synthesized by the hydrolysis of $Ti[OCH(CH_3)_2]_4$ as the precursor. These films have been utilized for the dissociation of phenol contaminant in water. Free-standing nanostructured film of silicon carbide (SiC) has been synthesized, employing a simple and new route of spray pyrolysis technique utilizing a slurry of Si in hexane. Another study is done on organized carbon nanotube (CNT) structures. These are made in the form of hollow cylinders (50 mm length, 4 mm diameter and 1.5 mm wall thickness). These CNT-based cylinders are made of conventional CNT and bamboo-shaped CNT. The filtrations of heavy hydrocarbons and *E. coli* bacteria from water have been carried out. In addition to this, ZnO nanostructures have also been studied. Another study concerns CNT–blood platelet clusters.

Keywords. Nanostructured TiO_2 film; photocatalytic degradation; SiC film; carbon nano-tube structures; ZnO structures.

PACS Nos 61.46.+w; 87.83.+a; 81.07.-b; 65.80.+n; 68.37.Lp; 68.37.Hk

1. Introduction

Nanostructure materials show lots of promise due primarily to the new and wide spectrum of properties exhibited by them. These are strikingly different from their bulk counterparts [1–8]. In this presentation, we will describe and discuss the synthesis, characterization and illustrated applications of some nanomaterials. TiO_2 is known to be a good photocatalytic material exhibiting significant stability in alkaline and acidic liquid media. In the present investigation we have synthesized nanostructured TiO_2 films through hydrolysis of titanium tetra-isopropoxide (TTIP) [9,10]. The nanocrystalline nature has been established through XRD, SEM and TEM techniques. The as-deposited film has been used as the electrode dipped

in the contaminated water containing phenol. On illumination with solar simulator (UV-rich visible light), it has been found that the interaction of photogenerated holes leads to the decomposition of phenol contaminant in the water. The disappearance of phenol has been monitored through the measurement of absorbance by UV–visible spectrophotometer. Silicon carbide is a well-known wide band-gap semiconductor with high breakdown electric field, high thermal conductivity and chemical inertness in oxidative or reductive media and strong mechanical properties [11,12]. Due to their unique properties of SiC in another study, free-standing silicon carbide films have been prepared through spray pyrolysis of silicon–hexane slurry. The formation of nanostructured silicon carbide films has been confirmed by employing XRD and SEM techniques.

We have synthesized self-organized structures of CNT (conventional and bamboo-shaped) forming macroscopic carbon cylinders of dimensions (50 mm length, ∼5 mm diameter, ∼1 mm thickness). We have used this bulk carbon cylinder as a filter to remove micro and nanoscale contaminants from water and heavy hydrocarbons from petroleum. ZnO has been shown to exhibit a variety of nanostructures (rods, stars, rings, belts, combs etc.) [13,14]. We have synthesized ZnO by evaporating Zn under oxygen–argon ambient. We have found that through suitable temperature profiles several nanostructures can be formed. Various nanoforms have been characterized by TEM and SEM. Through an exploratory study on CNT–blood platelet interaction, we have found that under suitable conditions, CNT acts as blocking sides which stops the blood platelet coagulation.

2. Experimental details, results and discussions

2.1 *TiO_2 nanostructured films*

The synthesis of nanostructured TiO_2 films has been done by sol–gel technique by the hydrolysis of titanium tetra-isopropoxide, which was deposited over transparent conducting oxide (TCO) and Ti substrates with spin coating technique (as shown in figure 1). The structural characterizations of the films were done through XRD. The XRD results shown in figure 2 revealed the formation of anatase phase (tetragonal, $a = 3.78$ Å and $c = 9.51$ Å) for TCO substrate while some rutile phases have also been seen for Ti substrates. As it can be seen in the SEM structure (figure 3), the mesoporous nanocrystalline TiO_2 deposited over different substrates, shows that the average particle size is ∼10–15 nm. The TEM microstructure is shown in figure 4, which revealed the formation of anatase phase with an average particle size of ∼2–10 nm. The TEM results are consistent with XRD and SEM results.

Photocatalytic degradation of phenol induced by UV-radiation using nanostructured TiO_2 films has been studied in the photocatalytic reactor $\sim 6 \times 4 \times 5$ cm^3 (cuboid in shape), which was made up of perspex sheets (a semi-transparent material) with holes on its two opposite faces. Over the central hole on one face of the photoreactor, quartz plate was mounted whereas the nanostructured TiO_2 film deposited over Ti-sheet with predefined area (e.g. 2×2 cm^2) was mounted on the opposite face of the photoreactor. UV-light was made to fall on TiO_2 nanostructured films through the quartz window. The space between quartz window and nanostructured TiO_2 films was filled with ∼50 ppm phenol solution (∼120 ml by

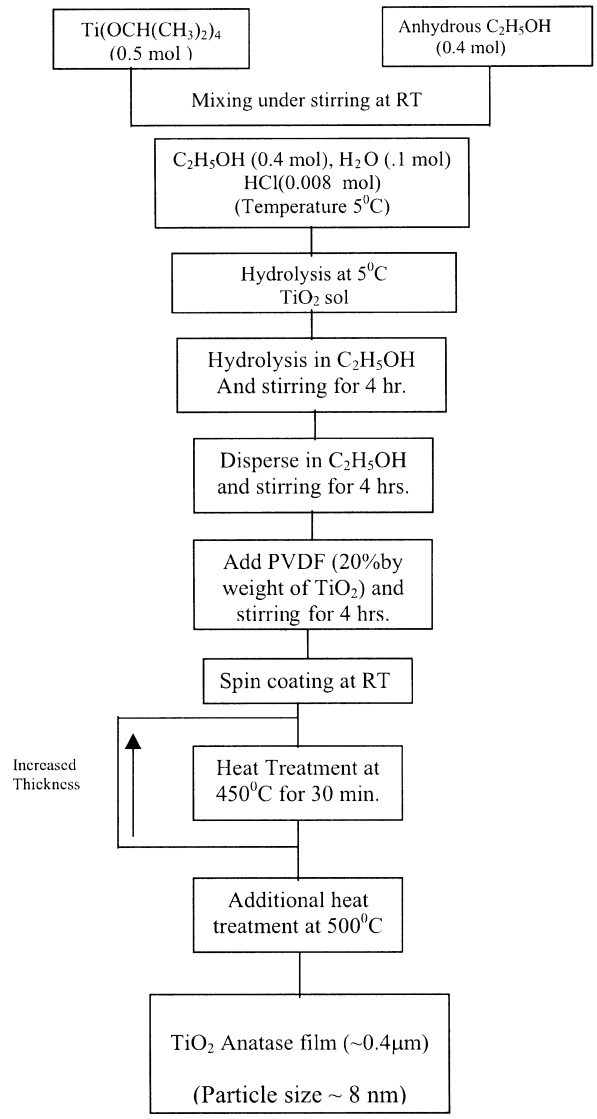

Figure 1. Steps involved in the synthesis of nanostructured TiO_2 films.

volume) prepared by dissolving phenol crystals in double distilled water. During the illumination, oxygen gas was purged into the solution with the help of porous fused silica tube by external cylinder. Overall assembly of the photocatalytic reactor for photocatalytic degradation of phenol is shown in figure 5. To determine the concentration of phenol in the solution, samples were collected after every 10-min interval upon UV-induced degradation of phenol. The concentration of phenol was determined by UV–visible absorption spectroscopic technique, where the absorbance was measured at a fixed wavelength (e.g. ∼269 nm) for all the samples.

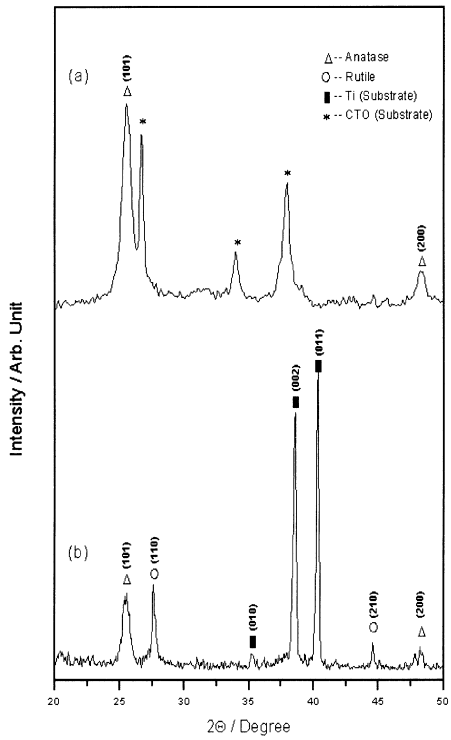

Figure 2. X-ray diffraction pattern of nanostructured TiO_2 film.

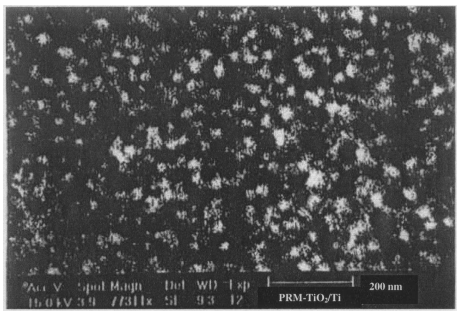

Figure 3. Scanning electron micrograph of the nanostructured TiO_2 film.

The possible mechanism for photocatalytic degradation of phenol using nanostructured TiO_2 as a photocatalyst is as follows [15]:

$$\mathrm{TiO_2(ns)} + h\nu \rightarrow e^- + h^+,$$
$$2\mathrm{H_2O} + h^+ \rightarrow \mathrm{H_2O^+} + \mathrm{H_2O} \rightarrow \cdot\mathrm{OH} + \mathrm{H_3O^+},$$
$$\mathrm{H_2O} + e^- \rightarrow \mathrm{H}\cdot + \mathrm{OH^-},$$
$$\mathrm{OH}\cdot + \cdot\mathrm{OH} \rightarrow \mathrm{H_2O_2},$$

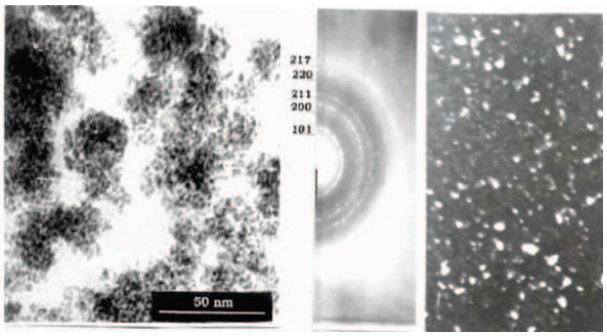

Figure 4. Transmission electron micrograph, selected area diffraction pattern and dark field image of (ns) TiO_2.

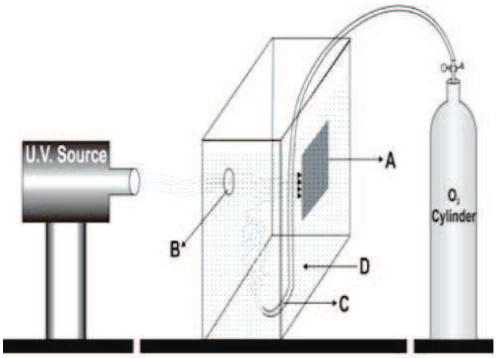

Figure 5. Arrangement for photocatalytic degradation of phenol employing nano-structured TiO_2 film. A – nanostructured TiO_2 film, B – quartz window, C – oxygen source, D – solution of phenol in water.

$$H_2O \rightarrow H_2O^* \rightarrow H_2O_2 + H_2,$$
$$\text{Phenol} + H_2O_2 \rightarrow \text{Products}.$$

The pH value of the phenol containing water after irradiation has been measured and plotted as a function of time of irradiation as shown in figure 6. Figure 7 shows the variation of phenol concentration with illumination time. These results show that the films of nanostructured TiO_2 upon illumination with UV-rich visible solar radiation have shown the significant degradation of phenol contaminants in the waste water.

2.2 *SiC nanostructured films*

Silicon powder (99.99%, particle size 0.05 mm) was ball-milled in an attritor ball mill at 400 rpm for 30 h in hexane medium. Milling the suspension of silicon in hexane resulted in the formation of slurry. This slurry was sprayed in a silica tube at a high temperature of 800–1000°C under argon atmosphere.

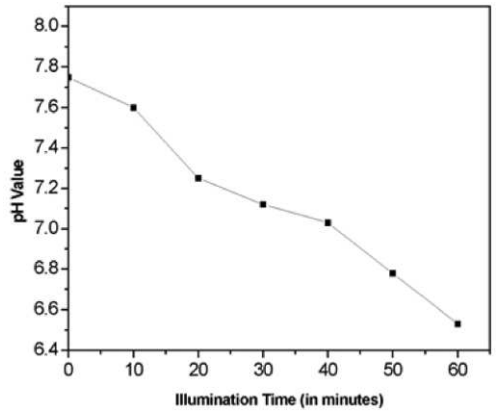

Figure 6. Variation of pH value of phenol with illumination time.

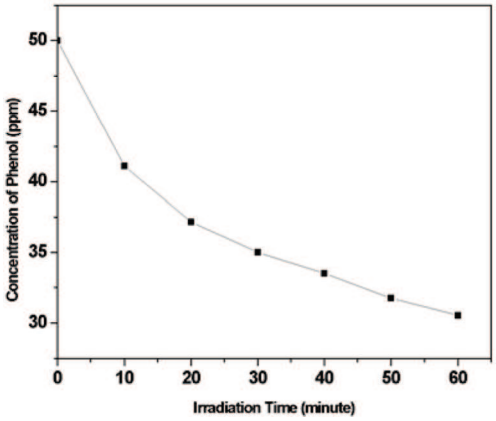

Figure 7. Variation of concentration of phenol with irradiation time.

Spray pyrolysis of suspended ball-milled silicon in hexane at 1000°C leads to homogenous film-like deposition. The as-deposited films could be easily detached from the tube and these free-standing films were characterized by XRD, SEM and TEM. Figure 8 shows a representative X-ray diffractogram of the as-deposited film. The analysis of the pattern reveals that the film corresponds to SiC. Based on XRD characterization it was found to be α-SiC (hexagonal; $a = 3.073$, $c = 15.08$). Some of the SiC reflections are indicated in figure 8. XRD patterns taken for several films invariably showed the formation of SiC.

The deposited films were easily detached from the silica tube and subjected to SEM. SEM study reveals the formation of nanocrystalline film of silicon carbide. Figure 9 shows the magnified SEM image of the as-deposited film, showing that the whole film is made up of nanocrystalline silicon carbide and the average size of the nanocrystals is 90–125 nm. Low magnification SEM micrograph of the film reveals the presence of some microspheres on the surface of the film (see figure 10).

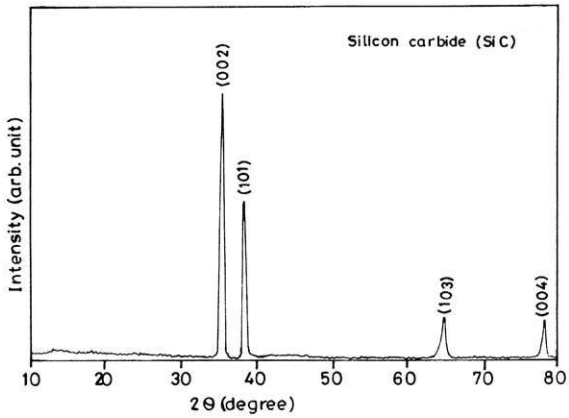

Figure 8. XRD pattern of the film obtained after spray pyrolysis of the milled silicon suspension in hexane at 1000°C in silica tube. The analysis of the XRD pattern reveals that the as-synthesized films correspond to α-SiC.

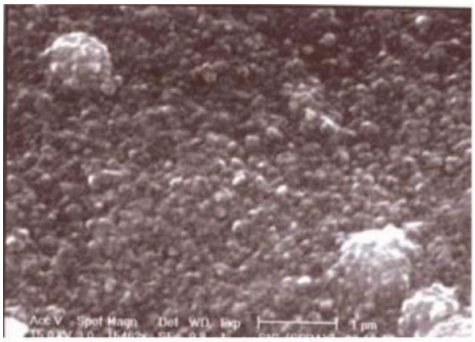

Figure 9. Magnified SEM micrograph of the film. This clearly shows that the SiC film is nanocrystalline and the size is ∼90–125 nm.

The size of the microspheres was ∼1 μm and these microspheres were also made up of the nanocrystalline SiC particles. Formation of microspheres is due to the agglomeration of the surface nanocrystals.

As described earlier, ball-milled silicon suspension in hexane has been sprayed in the silica tube at ≈1000°C in argon atmosphere. Due to the formation of nanocrystalline silicon by ball milling, the vaporization temperature will be lowered and the silicon will vaporize at the furnace temperature (1000°C). Hexane will apparently decompose. Therefore, enough number of silicon atoms and carbon atoms become available in the silica tube to the total heating zone of the furnace. These atoms will react and result in the formation of SiC. This will get deposited on the wall of silica tube, forming SiC nuclei. These will coalesce and agglomerate to form nanocrystalline silicon carbide film.

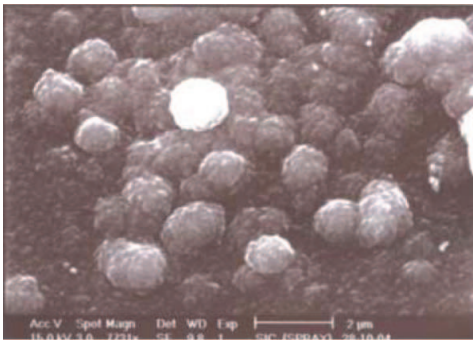

Figure 10. SEM micrograph showing microspheres of the size ∼1 μm observed at the surface of the film.

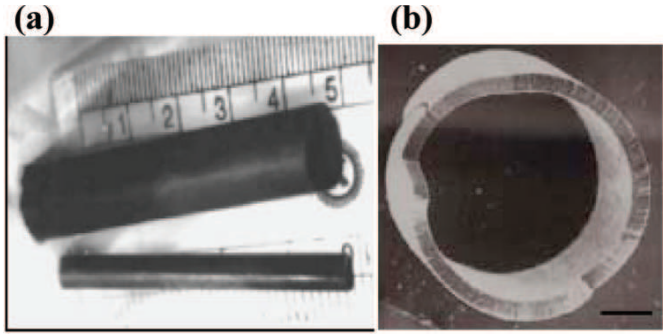

Figure 11. (**a**) Optical photograph of hollow carbon cylinders of length ∼5 cm and outer diameters 10 mm and 5.4 mm; (**b**) SEM micrograph of the radial aligned growth of CNT along the thickness constituting the bulk carbon hollow cylinder.

In order to check whether the as-synthesized SiC films contain some hydrogen, the films were annealed at ∼800°C for 6–10 h. No noticeable structural and/or microstructural changes could be seen as a result of annealing. This suggests that the as-grown SiC film do not contain hydrogen. Further investigations on this aspect are being carried out and the results will be forthcoming.

2.3 *Self-assembled CNT-based bulk carbon hollow cylinder*

We have synthesized macroscale hollow carbon cylinders up to centimeters in diameter and several centimeters long, with walls (ranging from 300 μm to 500 μm thick) consisting of micrometer length aligned multiwalled nanotubes (MWNTs). The aligned nanotubes that form uniform nanoporous, cylindrical membrane walls, are synthesized from sprayed ferrocene-derived iron catalyst particles; the nanotubes grow in radial directions on the walls of removable silica tube templates, leading to the formation of free-standing and continuous hollow cylindrical carbon tubes. Figure 11a shows the macroscale hollow carbon cylinders of length ∼5 cm

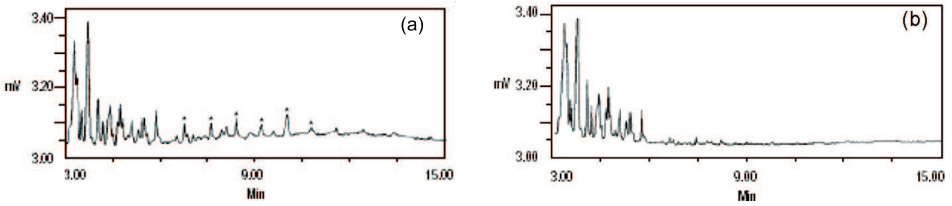

Figure 12. (**a**) Spectrum of the unifiltered products. The asterisks show the heavier hydrocarbon components in the unfiltered sample. (**b**) GC spectrum of the sample after it was passed through the nanotube filter, showing the absence of heavier hydrocarbon peaks.

and outer diameters 10 mm and 5.4 mm respectively. Figure 11b shows the SEM micrograph of the radial aligned growth of CNT along the thickness constituting the bulk carbon hollow cylinder. The length of the MWNTs corresponds to the wall thickness of the bulk structure. Figure 11b shows the dense packing of these aligned structures. The potential use of the nanotube-based macrostructure was explored in the filtration of heavier hydrocarbon species from hydrocarboneus oil and in the removal of bacteria from drinking water.

Figure 12a shows the gas chromatograph (GC) spectrum of the unfiltered gasolene. The asterisks show the heavier hydrocarbon components in the unfiltered sample. Figure 12b shows GC spectrum of the sample after it was passed through the nanotube filter, showing the absence of heavier hydrocarbon peaks.

To verify whether the filtration has taken place through the core or the interstitials of CNTs, we have synthesized the hollow cylinder consisting of bamboo-shaped carbon–nitrogen nanotubes [16]. The basic difference between this and the cylinder made up of conventional CNT is that the graphitic layers form a bamboo-like structure which blocks the core of the nanotube and only interstitials are left to pass the gasoline. A few experiments for the filtration of gasoline using bamboo-shaped CNT cylinder have been done and results will be forthcoming.

2.4 *ZnO nanostructures*

For growing ZnO nanoforms, we have used a two-zone furnace at temperatures 850°C and 350°C. The quartz tube of 3 cm diameter and 115 cm length has been used in which the furnace temperature is 850°C. The high purity Ar flow was switched on to a mixed gas stream of Ar = 0.5 l/m and O_2 = 0.3 l/m. Thus the Zn metal (300 mesh) was kept in an alumina boat and loaded in the central zone of the hot furnace at 850°C which was maintained throughout the whole reaction time (usually 10 min). The gas flow is stopped and both furnaces are switched off. Thus the furnace cool down to room temperature and white like products were observed in the tube. Depending upon the appearance of grown powders through the length of the quartz tube, three different batches of powders were collected and characterized by XRD (Phillips PW-1710) and SEM (Phillips XL-20). X-ray diffraction (XRD) characterization demonstrates that all the structural variants correspond to hexagonal wurtzite structured ZnO (figures 13a and 13b). Figures 14a and 14b

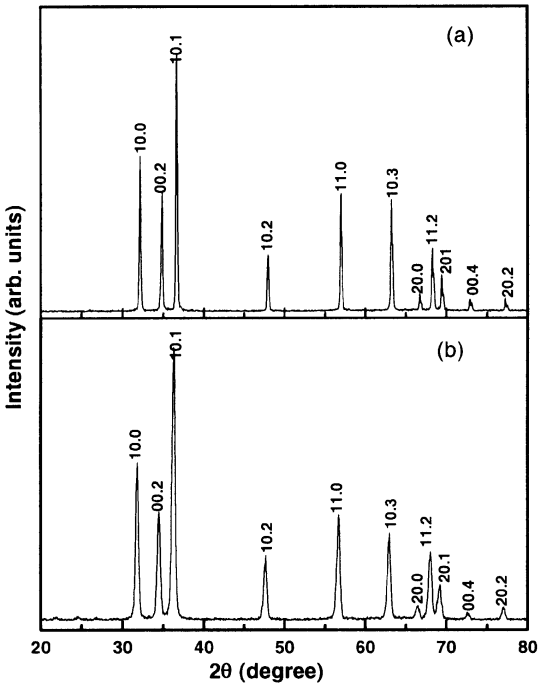

Figure 13a, b. X-ray diffraction patterns of ZnO nanostructure.

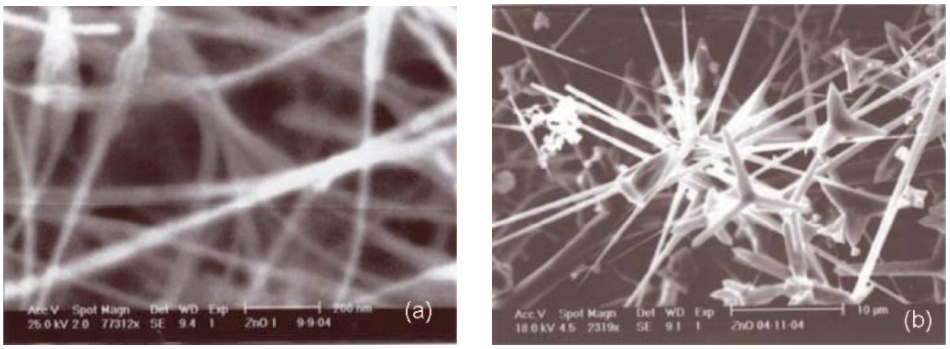

Figure 14a, b. Scanning electron micrograph from the different temperature zone showing nanowires and star nanorods.

are the scanning electron micrograph from the different temperature zone showing nanowires and star nanorods. Figure 15 shows the scanning electron micrograph of comb-like structures. ZnO is very rich in different morphology and exhibit lots of peculiar properties. We have expertise in growing different nanostructures and some structural property correlation measurements are in progress and their results are forthcoming.

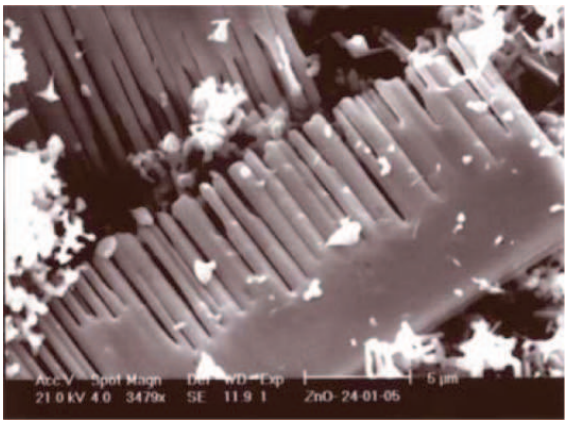

Figure 15. Scanning electron micrograph of comb-like structures.

2.5 *Carbon nanotubes–blood platelet clusters*

We have studied platelet reactivity by carbon nanotubes (MWNT). Carbon nanotubes were sonicated in an isotonic buffer with a Probe Sonicator. Platelets (from human blood) were suspended either in the presence or in the absence of carbon nanotubes. Platelets were stimulated with agonist peptides (10 μm) at 37°C under stirring condition (1200 rpm). Our preliminary experimental results show that there appears to be a fall in platelet reactivity to the stimulating agents, when the cells were suspended in the presence of carbon nanotubes.

3. Conclusions

Based on the present investigations, we arrived at the following conclusions:

(i) The nanostructured TiO_2 films have been synthesized by the hydrolysis of TTIP and effectively can be used for photocatalytic degradation of phenol under solar irradiation.

(ii) Spray pyrolysis of ball-milled silicon–hexane suspension leads to the formation of free-standing nanocrystalline SiC film.

(iii) Hollow bulk carbon cylinders made up of conventional carbon nanotubes and bamboo-shaped C-N nanotubes have been synthesized. These cylinders can be used to filter the heavier hydrocarbon from gasoline and bacteria from drinking water.

(iv) ZnO nanoforms have been grown using chemical vapor deposition techniques.

(v) Significant fall in platelet reactivity to the stimulating agents have been observed when the cells were suspended in the presence of carbon nanotubes.

Acknowledgements

The authors are extremely grateful to C N R Rao, A R Verma, S K Joshi, A K Raychoudhary, A K Sood, S N Upadhyay, R S Tiwari, A S K Sinha and P K Shukla for their encouragements and fruitful discussions. The authors are also grateful to Vijay Kumar (Scientific Officer) for technical assistance. Financial supports from DST (NSTI & UNANST), Council of Scientific and Industrial Research (CSIR), Ministry of Non-conventional Energy Sources (MNES) and the University Grants Commission (UGC), New Delhi, India are gratefully acknowledged.

References

[1] M Gratzel, *Nature (London)* **414**, 338 (2001)
[2] Z Zhang, C C Wang, R Zakaria and J Y Ying, *J. Phys. Chem.* **B102**, 10871 (1998)
[3] J J Biernacki and G P Wotzak, *J. Am. Ceram. Soc.* **72**, 122 (1989)
[4] G Shen, D Chen, K Tang, Y Qian and S Zhang, *Chem. Phys. Lett.* **375**, 177 (2003)
[5] C Ronning, P X Gao, Y Ding, Z L Wang and D Schwen, *Appl. Phys. Lett.* **84**, 783 (2004)
[6] Q Wan, C L Lin, X B Yu and T H Wang, *Appl. Phys. Lett.* **84**, 124 (2004)
[7] S Iijima, *Nature (London)* **354**, 56 (1991)
[8] M Terrones, R Kamalakaran, T Seger and M Rhle, *Chem. Commun.* **23**, 2335 (2000)
[9] P R Mishra, P K Shukla, A K Singh and O N Srivastava, *Int. J. Hydrogen Energy* **28**, 1089 (2003)
[10] B O'Regan and M Gratzel, *J. Phys. Chem.* **94**, 8720 (1990)
[11] F Liao, S Park, J M Larson, M R Zachariah and S L Girshick, *Mater. Lett.* **57**, 1982 (2003)
[12] V Yong and H T Hahn, *Nanotechnology* **15**, 1338 (2004)
[13] Z L Wang, *Mater. Today* **7**, 26 (2004)
[14] F Liu, P J Cao, H R Zhang, J Q Li and H J Gao, *Nanotechnology* **15**, 949 (2004)
[15] J Gao, Z Hu, X Wang, J Hou and Q Lu, *Plasma Sci. Technol.* **3**, 765 (2001)
[16] Ram Manohar Yadav, Anchal Srivastava and O N Srivastava, *J. Nanosci. Nanotech.* **3**, 223 (2003)